


## Article

# Chemical Modification of B<sub>4</sub>C Films and B<sub>4</sub>C/Pd Layers Stored in Different Environments

Yufei Feng <sup>1</sup>, Runze Qi <sup>1,\*</sup>, Li Jiang <sup>1</sup>, Qiushi Huang <sup>1</sup> , Tongzhou Li <sup>1</sup>, Genchang Liu <sup>1</sup>, Wenbin Li <sup>1</sup>, Wensheng Yan <sup>2</sup>, Zhong Zhang <sup>1</sup> and Zhanshan Wang <sup>1</sup>

<sup>1</sup> MOE Key Laboratory of Advanced Micro-Structured Materials, Institute of Precision Optical Engineering (IPOE), School of Physics Science and Engineering, Tongji University, Shanghai 200092, China; 1810089@tongji.edu.cn (Y.F.); 1986jiangli@tongji.edu.cn (L.J.); huangqs@tongji.edu.cn (Q.H.); litongzhou@tongji.edu.cn (T.L.); liugenchang@tongji.edu.cn (G.L.); wbli@tongji.edu.cn (W.L.); zhangzhongcc@tongji.edu.cn (Z.Z.); wangzs@tongji.edu.cn (Z.W.)

<sup>2</sup> National Synchrotron Radiation Laboratory, University of Science and Technology of China, Hefei 230029, China; ywsh2000@ustc.edu.cn

\* Correspondence: qrz@tongji.edu.cn; Tel.: +86-6598-4652

**Abstract:** B<sub>4</sub>C/Pd multilayers with small d-spacing can easily degrade in the air, and the exact degradation process is not clear. In this work, we studied the chemical modification of B<sub>4</sub>C films and B<sub>4</sub>C/Pd double layers stored in four different environments: a dry nitrogen environment, the atmosphere, a dry oxygen-rich environment, and a wet nitrogen environment. The XANES spectra of the B<sub>4</sub>C/Pd layers placed in a dry oxygen-rich environment showed the most significant decrease in the  $\sigma^*$  states of the B–C bonds and an increase in the  $\pi^*$  states of the B–O bonds compared with the other samples. X-ray photoelectron spectroscopy (XPS) measurements of the samples placed in a dry oxygen-rich environment showed more intensive B–O binding signals in the B<sub>4</sub>C/Pd layers than in the single B<sub>4</sub>C film. The results of the Fourier-transform infrared spectroscopy (FTIR) showed a similar decrease in the B–C bonds and an increase in the B–O bonds in the B<sub>4</sub>C/Pd layers in contrast to the single B<sub>4</sub>C film placed in a dry oxygen-rich environment. We concluded that the combination of palladium catalysis and the high content of oxygen in the environment promoted the oxidization of boron, deteriorated the B<sub>4</sub>C composition.

**Keywords:** B<sub>4</sub>C film; B<sub>4</sub>C/Pd layers; catalysis; storage environment; XANES



**Citation:** Feng, Y.; Qi, R.; Jiang, L.; Huang, Q.; Li, T.; Liu, G.; Li, W.; Yan, W.; Zhang, Z.; Wang, Z. Chemical Modification of B<sub>4</sub>C Films and B<sub>4</sub>C/Pd Layers Stored in Different Environments. *Materials* **2021**, *14*, 1319. <https://doi.org/10.3390/ma14051319>

Academic Editor: Christian Müller

Received: 2 February 2021

Accepted: 3 March 2021

Published: 9 March 2021

**Publisher's Note:** MDPI stays neutral with regard to jurisdictional claims in published maps and institutional affiliations.



**Copyright:** © 2021 by the authors. Licensee MDPI, Basel, Switzerland. This article is an open access article distributed under the terms and conditions of the Creative Commons Attribution (CC BY) license (<https://creativecommons.org/licenses/by/4.0/>).

## 1. Introduction

The photon flux of multilayer monochromators on synchrotron beamlines is approximately two orders of magnitude larger than that of crystal monochromators [1,2]. The most distinct advantage of these techniques is that they do not require high energy resolution, such as X-ray fluorescence spectroscopy (XRF) [3,4], small-angle X-ray scattering (SAXS) [5,6], and X-ray micro-imaging [7,8]. There are many typical multilayer material combinations for monochromators, for example, Si/W [9,10], B<sub>4</sub>C/W [4,11,12], and B<sub>4</sub>C/Pd [8,13,14]. B<sub>4</sub>C/Pd multilayers, which have high reflectivity and good energy resolution at approximately 7–15 keV, have been used in synchrotron beamlines, such as TopoTomo (ANKA light source) [14]. Recently, Ni et al. have fabricated the ultrathin B<sub>4</sub>C/Pd multilayers with d-spacing of 2.5 nm by magnetron sputtering using the heavy noble gas Kr to improve the layer structure [15]. The excellent performance of B<sub>4</sub>C/Pd multilayers are suitable to be used as a monochromator.

However, small d-spacing B<sub>4</sub>C/Pd multilayers are unstable under an atmospheric environment. Morawe et al. reported that B<sub>4</sub>C/Pd multilayers with d-spacing of approximately 3 nm degraded in the air after only a few days without protective layers [16,17]. The first peak of measured X-ray reflectivity curve broadened and shoulders appeared at higher angles indicating the compaction of the B<sub>4</sub>C layers and destruction of the periodic

structure. With larger d-spacing, multilayers deposited by reactive sputtering using an Ar and N<sub>2</sub> gas mixture were also unstable compared to other nitridated multilayers, like B<sub>4</sub>C+N/Ru [18,19] and B<sub>4</sub>C+N/W multilayers [20]. Wang et al. reported that nitridated B<sub>4</sub>C/Pd multilayers with d-spacing of approximately 5 nm decayed after the samples were stored in an air environment for 6–17 months [21].

We found that many layers near the surface deteriorated with severe interdiffusion and compaction of the layers. This is a significant issue for applications, as most multilayers for hard X-ray monochromator have d-spacing less than 3 nm, and the conditions for preparation, storage, and installation become critical. Although certain protective layers have been developed to elongate the lifetime of B<sub>4</sub>C/Pd multilayers [16], there is no further investigation of the effects of different environmental factors, the contribution from different materials, and the composition changes of films in the degradation process, which is essential for the future development and applications of B<sub>4</sub>C/Pd multilayer monochromators.

The oxidation of B<sub>4</sub>C as an important subject has been studied in many literatures. Zehringer et al. [22] reported that exposure of sputter-cleaned surfaces of boron-carbide to molecular oxygen at room temperature did not cause a measurable surface oxidation. Li et al. [23] found Gibbs energy of the reaction between B<sub>4</sub>C and oxygen was great than that of the reaction between B<sub>4</sub>C and water vapor at the same temperature. Viricelle et al. [24] reported that the oxidation rate of B<sub>4</sub>C increases and is enhanced by water vapor at 700 and 800 °C. To sum up, B<sub>4</sub>C is very stable at room temperature, and will oxidize with oxygen and water at a high temperature.

Palladium is typically used as a catalyst in chemistry. Nicolaou et al. reported that palladium catalyzed carbon-carbon bond formation in most common synthesis reactions [25]. Tat Thang Vo Doan et al. [26] and Li et al. [27] found that B-Pd nanocrystals reduced O=O bond reaction barriers and strengthened oxygen reduction reactions. Palladium catalysis promotes the dissociation of oxygen and reduces the oxidation reaction potential. Therefore, we can assume that the presence of Pd promotes B<sub>4</sub>C oxidation.

In this paper, we first confirm the hypothesis of the catalytic effect of Pd on B<sub>4</sub>C/Pd layered systems and further explore the degradation process by investigating the stability of B<sub>4</sub>C films and B<sub>4</sub>C/Pd double layers stored in different environments. We fabricated two groups of samples of a single B<sub>4</sub>C film and a B<sub>4</sub>C layer with a Pd layer underneath. Both groups of samples were placed in different environments for 50 days. The samples were then measured using X-ray absorption near-edge structure (XANES) spectroscopy, X-ray photoelectron spectroscopy (XPS), and Fourier-transform infrared spectroscopy (FTIR) to analyze the changes in the chemical state after film degradation. The results indicated that boron combined with oxygen and boron carbide degraded under the action of palladium in the oxygen environment. The work is a useful guide for exploring the oxidation process of B<sub>4</sub>C materials with nano-film state, and for the protection and application of ultrathin B<sub>4</sub>C/Pd multilayers in synchrotron monochromators.

## 2. Experimental Techniques

### 2.1. Sample Preparation

The direct current (DC) magnetron sputtering technique was developed to prepare samples. Each magnetron cathode was operated at 100 W and 15 W for the B<sub>4</sub>C and Pd targets, respectively. The samples were deposited at Ar gas pressures of 1 mTorr at room temperature and the background pressure was lower than  $5.5 \times 10^{-5}$  Pa to avoid the incorporation of oxygen into the sputtering process. Firstly, the deposition rate of B<sub>4</sub>C and Pd was calibrated by measuring and fitting the X-ray reflectivity curve of single B<sub>4</sub>C and Pd films. Known from our previous investigation [28], the stoichiometric ratio of B:C was around 4:1 as the B<sub>4</sub>C layer sputtered at Ar gas pressures of 1 mTorr. The thin B<sub>4</sub>C film obtained under this sputtering condition is very dense, with a density (2.39 g/cm<sup>3</sup>) equivalent to 95% of the bulk B<sub>4</sub>C material (2.52 g/cm<sup>3</sup>). Then two groups of samples were fabricated. In the first group of samples, a 10 nm B<sub>4</sub>C film was deposited directly on a Si substrate. In the second group, a 1 nm Pd layer was added between a 10 nm B<sub>4</sub>C layer and

a Si substrate to prove the function of Pd. After preparation, the samples were immediately transferred to the corresponding storage environment.

## 2.2. Storage Environment Conditions

To explore the factors that degrade films, the B<sub>4</sub>C films and B<sub>4</sub>C/Pd layers were sealed in boxes and stored in four different environments for 50 days: (A) A dry nitrogen environment (pumped down and filled with nitrogen), which is isolated from O<sub>2</sub> and H<sub>2</sub>O and can be used as a reference. (B) The atmosphere, which is the assumed working environment of the optics. (C) A dry oxygen-rich environment (pumped down and filled with oxygen), where oxygen is the impact factor. (D) A wet nitrogen environment (pumped down, humidified, and filled with nitrogen), where H<sub>2</sub>O is the impact factor. Detailed parameters of the storage environments are listed in Table 1. The samples stored in a dry nitrogen environment, isolated from O<sub>2</sub> and H<sub>2</sub>O, can be used as a reference.

**Table 1.** Detailed parameters of the storage environments.

Environments	Temperature/°C	Humidity/%rh
A: Dry nitrogen environment	20 °C	~25%rh
B: Atmosphere	20 °C	~35%rh
C: Dry oxygen-rich environment	20 °C	~25%rh
D: Wet nitrogen environment	20 °C	~85%rh

## 2.3. The X-ray Absorption Near-Edge Structure (XANES)

X-ray absorption near-edge structure (XANES) spectroscopy is commonly used to probe the local atomic structure around specific elements in films and often used as a fingerprint of the changes in the coordination numbers of elements [29–33]. XANES measurements were conducted 50 days after fabrication at the Beamline U12b at the National Synchrotron Radiation Laboratory (NSRL) in the total electron yield (TEY) mode by collecting sample drain currents under a vacuum at greater than  $5 \times 10^{-8}$  Pa. The beam from a bending magnet was monochromatized with a varied line-spacing plane grating and refocused using a toroidal mirror. An energy range from 100 to 1000 eV was used with an energy resolution of approximately 0.2 eV [34].

All XANES spectra were measured using the process of background subtraction and normalization by considering the low and high photon energy parts of the spectra far from the threshold [32].

## 2.4. X-ray Photoelectron Spectroscopy (XPS)

To study the changes in the electronic structures of the films' elements after degradation, the XPS measurements were conducted using a Thermo Fisher Scientific K-Alpha+ spectrometer (Thermo Fisher Scientific, Waltham, MA, USA) with an Al-K $\alpha$  characteristic emission line (photon energy  $E = 1486$  eV) [35]. The B 1s, C 1s, and O 1s core-level spectra were investigated after the single B<sub>4</sub>C films and B<sub>4</sub>C/Pd layers were placed in the dry oxygen-rich environment. The Pd 3d core-level spectra at the interface of the Pd and B<sub>4</sub>C layers were also investigated to explore the chemical state of Pd.

## 2.5. Fourier-Transform Infrared Spectroscopy (FTIR)

Fourier-transform infrared spectroscopy was recorded on a Fourier-transform infrared spectrometer (FTIR, Tensor 27). First, a spectrum of the Si substrate was collected as the background spectrum. The spectra of the single B<sub>4</sub>C films and B<sub>4</sub>C/Pd layers placed in the dry oxygen-rich environment were then obtained under the same test conditions. The data processing consisted of two steps: Background subtraction and position correction based on the peaks of the Si–Si bonds [36].

### 3. Experimental Results

#### 3.1. XANES Measurements

##### 3.1.1. B K-Edge XANES

The B K-edge X-ray absorption near-edge structure spectra of the samples placed in the different storage environments are shown in Figure 1. The spectra had three features: One peak at 191.6 eV, one minor sharp oscillation at 193 eV, and one broad slope from 196.0 eV to 208.0 eV that were marked as a, b, and c, respectively. The spectral features at the different energy positions represented different chemical states and the local atomic structure of boron. Peak a at 191.6 eV was due to the transition of B 1s electrons to unoccupied B 2p states of  $B_4C$  [37]. Feature b at 193 eV was attributed to the localized  $\pi^*$  states of  $B_2O_3$  [37–39], and the broad feature c from 196.0 eV to 208.0 eV was due to the  $\sigma^*$  states of the B–C bonds [38–41]. As shown in Figure 1a, the three spectral features of the B1, C1, and D1 samples of the single  $B_4C$  films underwent no significant changes compared with the A1 sample placed in the dry nitrogen environment.

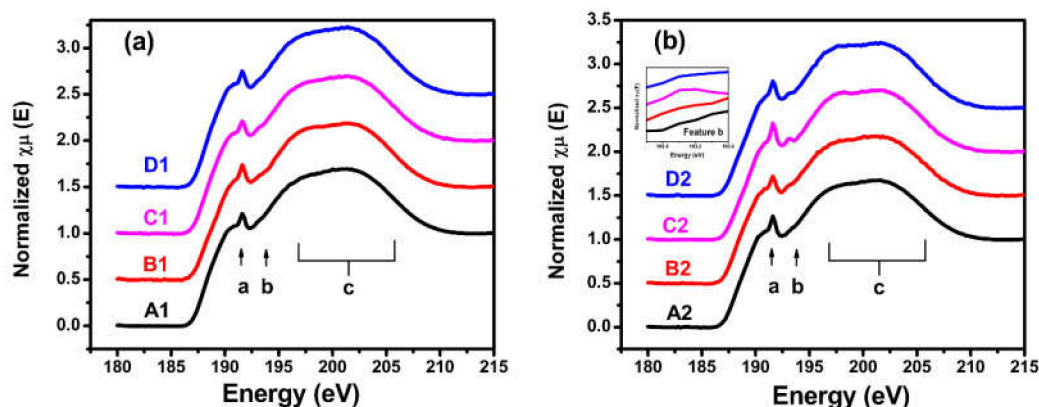


**Figure 1.** The B K-edge X-ray absorption near-edge structure (XANES) spectra of the  $B_4C$  films (a) and  $B_4C/Pd$  layers (b) in the different storage environments. Samples A1 and A2 were placed in a dry nitrogen environment; samples B1 and B2 were placed in the atmosphere; samples C1 and C2 were placed in a dry oxygen-rich environment; and samples D1 and D2 were placed in a wet nitrogen environment. The insert in Figure 1b is an enlarged view of feature b in the  $B_4C/Pd$  layers.

The results indicate that the local atomic structure around the boron experienced almost no changes in the single  $B_4C$  films even in the different environments. Figure 1b shows that the three spectral features of the  $B_4C/Pd$  layers placed in the dry oxygen-rich environment (C2 sample) changed significantly compared with the A2 sample placed in the dry nitrogen environment. Peak a at 191.6 eV in the C2 sample's spectrum was more intense and sharper than the other samples, indicating that some boron atoms became unstable in the  $B_4C/Pd$  layers placed in the dry oxygen-rich environment.

The peak position of feature b was related to the  $\pi^*$  states of the  $B_2O_3$ , suggesting that some of the boron combined with oxygen. This change agreed with the results of the O K-edge XANES presented in Figure 4, with peaks at 536.1 eV [39,42,43]. The decline in feature c, assigned to the  $\sigma^*$  states of the B–C bonds, indicated that some B–C chains were breaking in the film [38,39]. The corresponding change also appeared in the C K-edge XANES signal with a peak at 284.5 eV and a slope from 291 to 298 eV [40,41] as shown in Figure 3. These spectral features demonstrated that, in the  $B_4C/Pd$  layers placed in the oxygen-rich environment, the local atomic structure and chemical states of the boron changed.

The spectral features of the  $B_4C/Pd$  layers placed in the atmosphere and wet nitrogen environment (the B2 and D2 samples, respectively) changed little compared with the  $B_4C/Pd$  layers placed in the dry nitrogen environment (A2 sample). There was almost no increase in the B2 sample's spectrum due to the low concentration of oxygen in the atmosphere. As no obvious changes were observed in the D2 sample's spectrum,  $H_2O$  appeared to have less effect on the degradation of the layers compared to  $O_2$ .

To further prove the effects of palladium and oxygen on the degradation of the films, the spectra of different films in the same storage environments are demonstrated in Figure 2. Figure 2a shows the spectra of the single B<sub>4</sub>C film and B<sub>4</sub>C/Pd layers placed in the dry nitrogen environment. There was no obvious difference in the spectral features between the two samples, proving that the B<sub>4</sub>C/Pd layers were stable without the action of oxygen. Figure 2b shows the spectra of the single B<sub>4</sub>C film and the B<sub>4</sub>C/Pd layers placed in the dry oxygen-rich environment. The spectral features, as previously mentioned, of the B<sub>4</sub>C/Pd layers showed obvious changes, indicating that the presence of palladium degraded the film in the dry oxygen-rich environment.

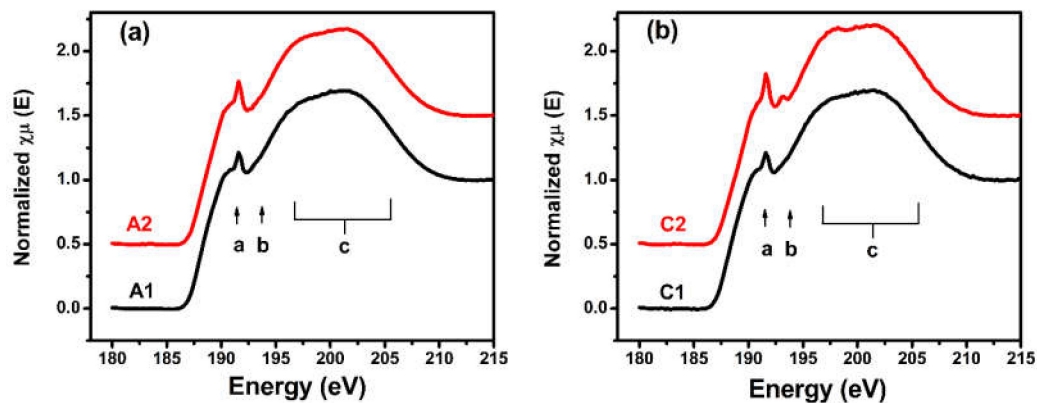


**Figure 2.** The B K-edge XANES spectra of the B<sub>4</sub>C films (A1 and C1) and B<sub>4</sub>C/Pd layers (A2 and C2) placed in the dry nitrogen environment (a) and in the dry oxygen-rich environment (b).

### 3.1.2. C K-Edge XANES

The C K-edge X-ray absorption near-edge structure spectra were measured to analyze the change of local atomic structure around the carbon element. Figure 3 shows the C K-edge X-ray absorption near-edge structure spectra of the different films placed in the dry oxygen-rich environment. The C 1s absorption edge of the B<sub>4</sub>C film was characterized by the antibonding  $\pi^*$  state of the C–B bonds at 284.5 eV and the  $\sigma^*$  states of the C–B bonds from 291 to 298 eV, symbolized by d and e, respectively [40,41]. The most significant change in the C 1s spectrum of the B<sub>4</sub>C/Pd layers was the decrease in the intensity of the antibonding  $\pi^*$  state and the  $\sigma^*$  state compared with the spectrum of the B<sub>4</sub>C film. The decrease proved that the part of C–B chain was breaking due to the presence of Pd in the oxygen-rich environment and as a result, part of the B<sub>4</sub>C composition was destroyed.

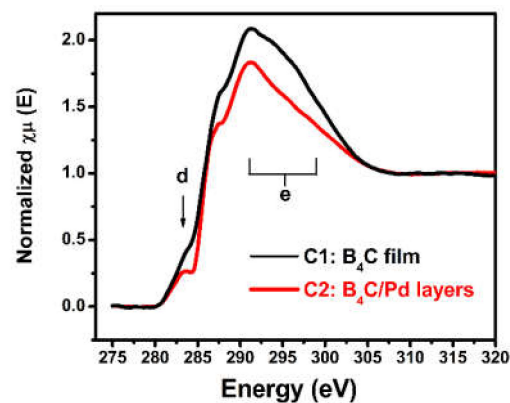


**Figure 3.** The C K-edge XANES spectra of the B<sub>4</sub>C film and B<sub>4</sub>C/Pd layers placed in the dry oxygen-rich environment.

### 3.1.3. O K-Edge XANES

To prove the effect of oxygen on the film, the O K-edge X-ray absorption near-edge structure spectra were also measured. Figure 4 displays the O K-edge X-ray absorption near-edge structure spectra of the different films placed in the dry oxygen-rich environment. The spectra had two significant features: one small bump due to the  $\pi^*$  state of the  $O_2$  molecule at 529.5 eV [42–45], labeled f, and another broad feature attributed to the  $\sigma^*$  state of the B–O bonds at 536.1 eV [43–45], labeled g. There was a significant increase in the  $\sigma^*$  states of the B–O bonds in the spectrum of the  $B_4C/Pd$  layers compared with the spectrum of the  $B_4C$  film, which indicated that some of the oxygen was excited and combined with boron under palladium catalysis. The same  $O_2$  peak occurred in the spectra because the samples were placed in a dry oxygen-rich environment.

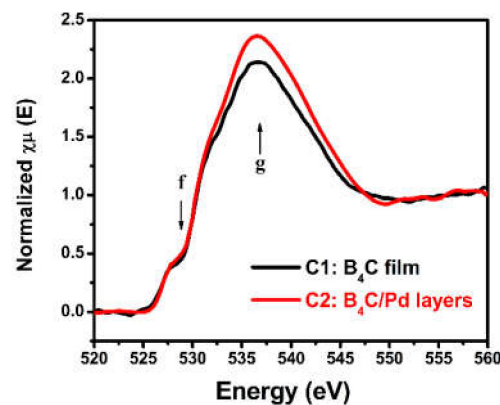


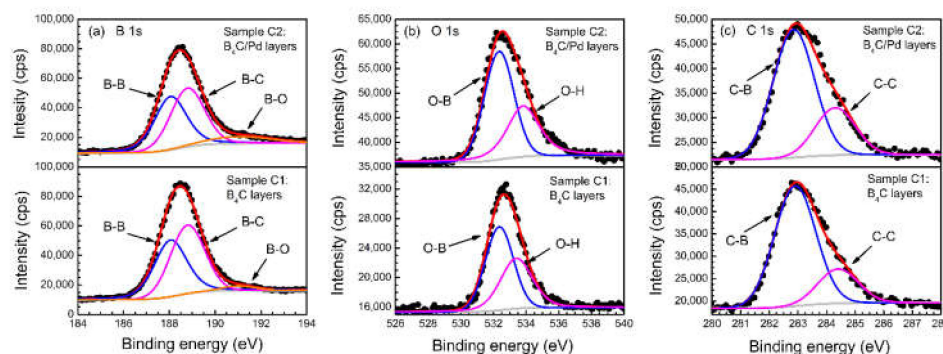
**Figure 4.** The O K-edge XANES spectra of the  $B_4C$  film and  $B_4C/Pd$  layers placed in the dry oxygen-rich environment.

Summarizing the XANES results, there was a reasonable explanation of the degradation of the  $B_4C/Pd$  layers: Under palladium catalysis, some of oxygen was excited [27], replacing some of the carbon atoms around the boron and combining with the boron, which caused the deterioration of the  $B_4C$  composition.

### 3.2. XPS Measurements

Examinations of the XPS spectra around the B 1s, O 1s, C 1s, and Pd 3d regions provided more details about the electronic structures of the film elements. Figure 5 presents the B 1s, O 1s, and C 1s spectra of the single  $B_4C$  film and  $B_4C/Pd$  layers placed in the dry oxygen-rich environment. Both test positions were approximately 5 nm from the surface of the  $B_4C$  layer to avoid surface contamination. All photoelectron peaks were fitted by a weighted least-squares fitting method using Lorentzian–Gaussian line shapes after background subtraction according to the Shirley method. The peak width of the fitted spectra of  $B_4C$  film was consistent with the  $B_4C/Pd$  layers.

Figure 5a presents the B 1s spectra of the single  $B_4C$  film and  $B_4C/Pd$  layers. In the spectrum of the  $B_4C/Pd$  layers, there was a weak slope at a binding energy of 192.5 eV due to the B–O component [27,46,47], which indicated that some of the boron (~9% in atomic fraction) combined with oxygen under the action of palladium. A small B–O component (~2% in atomic fraction) was also found by fitting the B 1s spectra of the single  $B_4C$  film. The B 1s spectra also show the reduction of B–B bonds (from about 48% down to 45% in the atomic fraction) and B–C bonds (from about 50% down to 46% in the atomic fraction) at binding energies of 188 and 189 eV, respectively [46–48].



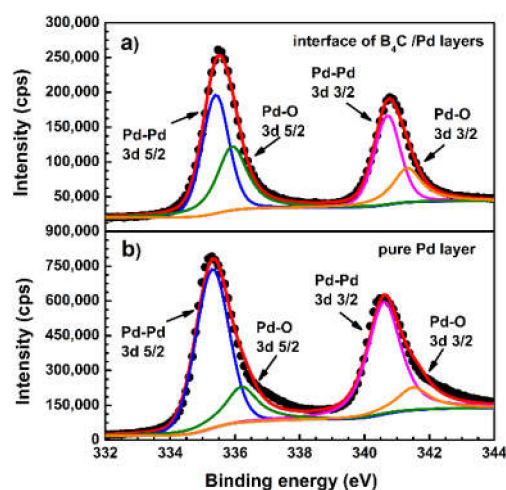
**Figure 5.** The X-ray photoelectron spectroscopy (XPS) spectra of the  $B_4C$  film and  $B_4C/Pd$  layers placed in the dry oxygen-rich environment. (a) B 1s, (b) O 1s, and (c) C 1s.

Figure 5b shows the O 1s spectra of the single  $B_4C$  film and  $B_4C/Pd$  layers. The signal peak was due to the O–B bonds at 531.7 eV [49] and the O–H bonds at 533.2 eV [50] from the adsorbed water molecules. The amount of O–B bonds in the spectrum of the  $B_4C/Pd$  layers (~58% in the atomic fraction) were higher than in the spectrum of the single  $B_4C$  film (~54% in the atomic fraction). The results indicate that a larger ratio of oxygen reacted with boron under the presence of palladium, which is consistent with the results of the B 1s spectra. The stoichiometric ratio of O:B was around 1:9.8 in the  $B_4C/Pd$  layers, which was larger than in the single  $B_4C$  films (1:18.8). This shows that the content of oxygen in the  $B_4C/Pd$  layers significantly increased under the catalysis of palladium. The results also indicate that the amount of oxidized boron in the  $B_4C/Pd$  layers increased significantly.

Figure 5c demonstrates the XPS spectra of C 1s in the single  $B_4C$  film and  $B_4C/Pd$  layers. The C 1s spectra had peaks at binding energies of 283.0 eV and 284.5 eV due to the C–B bonds and C–C bonds, respectively [46–48]. There was a reduction in the C–B bonds in the spectrum of the  $B_4C/Pd$  layers (~66% in atomic fraction) compared with those in the spectrum of the  $B_4C$  film (~71% in atomic fraction), indicating that some of the C–B bonds broke due to the reaction of B with O in the  $B_4C/Pd$  layers. This result was consistent with the C K-edge XANES analysis.

To further explore the changes of palladium, the XPS spectra of Pd 3d were also measured. Figure 6a shows the XPS spectrum of the Pd 3d at the interface of the  $B_4C/Pd$  layers placed in the dry oxygen-rich environment. The spectrum of the Pd 3d at the position approximately 5 nm from the surface of single Pd layer, as reference, is also shown in Figure 6b. All photoelectron peaks were fitted by a weighted least-squares fitting method using Lorentzian–Gaussian line shapes after background subtraction according to the Shirley method. In the spectrum of the pure Pd layer, the peak was fitted as the 3d 5/2 and 3d 3/2 levels of the Pd–Pd bonds located at 335.3 eV and 340.6 eV [27,51,52], and a small portion of the 3d 5/2 and 3d 3/2 levels of the Pd–O bonds located at 335.9 eV and 341.3 eV [27,51,52]. The atomic fraction of the Pd–O bonds was about 21%.

For the spectrum of the Pd 3d at the interface of the  $B_4C/Pd$  layers placed in the dry oxygen-rich environment, the peaks were slightly shifted to a higher energy position due to the enhancement of the Pd–O bonds signal. The atomic fraction of the Pd–O bonds was about 39%. The increase of the Pd–O bonds indicates that more Pd atoms were excited. Therefore, Pd will be more involved in the reaction in the  $B_4C/Pd$  layers placed in the dry oxygen-rich environment. The same result also appeared in other Pd catalytic experiments [26,27], demonstrating that, when Pd, B, and O coexist, Pd donates electrons to O and B transfers electrons to O, indicating that Pd and B are involved in the decomposition of O and promotes oxygen reduction reactions.



**Figure 6.** The XPS spectra of the Pd 3d: (a) at the interface of the Pd layer and  $B_4C$  layer placed in the dry oxygen-rich environment; and (b) pure Pd layer.

### 3.3. FTIR Absorption Spectra

To further investigate the vibration of bonds, the FTIR absorption spectra were recorded. Figure 7 shows the FTIR absorption spectra of the single  $B_4C$  film and  $B_4C/Pd$  layers placed in the dry oxygen-rich environment. The spectrum of the  $B_4C$  film had a strong absorption peak near  $1100\text{ cm}^{-1}$  that was due to the B–C bonds in the  $B_4C$  composition [53–56]. In the spectrum of the  $B_4C/Pd$  layers, the peak of the B–C bonds decreased significantly, indicating that some of B–C chains were breaking due to the presence of the Pd in the oxygen-rich environment. In addition, there were two new peaks in the spectrum of the  $B_4C/Pd$  layers, minor features in the regions of  $950\text{--}1000\text{ cm}^{-1}$ , and absorption bands in the regions of  $1200\text{--}1300\text{ cm}^{-1}$  due to the B–O modes [54–56], indicating that some of the boron was oxidized. The FTIR absorption spectra confirmed that part of  $B_4C$  composition was destroyed and that boron combined with oxygen in the dry oxygen-rich environment under palladium catalysis.

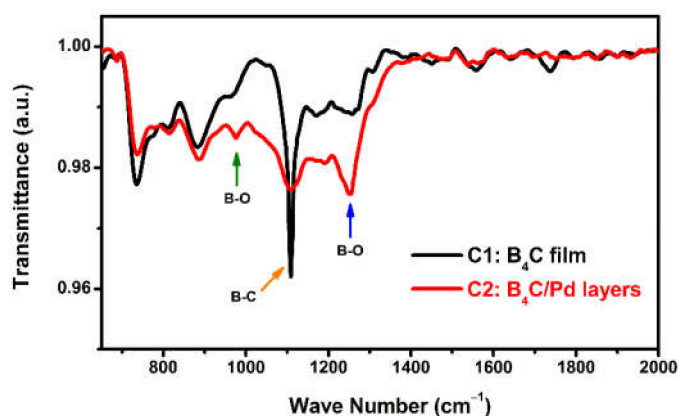


**Figure 7.** The Fourier-transform infrared spectroscopy (FTIR) absorption spectra of the  $B_4C$  film and  $B_4C/Pd$  layers placed in the dry oxygen-rich environment.

## 4. Discussion

The three measurements showed the same results indicating that the  $B_4C$  composition tended to degrade under palladium catalysis in the oxygen environment. Considering that the film is only a few nanometers, these characterizations are enough to clearly prove the effect of Pd and O on this degradation process. A simple degradation process could be assumed as follows:



1. First oxygen diffused into the film. Known from the previous calculation of density functional theory (DFT), O<sub>2</sub> dissociation proceeds on a Pd layer with reaction barriers of 0.72 eV [26]. The energy of the reaction barriers decreases to 0.63 eV when B and Pd exist simultaneously [26], indicating B and Pd enhance the decomposition of O and promote the oxidation reaction. In our work, the most obvious structural change occurs in the B<sub>4</sub>C/Pd layers placed in a dry oxygen-rich environment. In this case, it is essential that numerous O<sub>2</sub> will decompose into O with the participation of B and Pd.
2. Then, dissociated oxygen replaced the carbon around boron and combined with boron. The formation of B<sub>2</sub>O<sub>3</sub> ( $\Delta_f H^\circ = -1194$  kJ/mol) releases a larger amount of energy than B<sub>4</sub>C ( $\Delta_f H^\circ = -71$  kJ/mol) [16], indicating that boron prefers to combine with oxygen. In other B<sub>4</sub>C oxidation experiments [23], at elevated temperatures, carbon atoms will form carbon dioxide. While in our experiment, at room temperature, carbon atoms can only be in a non-excited state [17]. Thus, we could assume that the reaction product prefers boron oxide and carbon.
3. Finally, if water vapor exists, B<sub>2</sub>O<sub>3</sub> will react to form H<sub>3</sub>BO<sub>3</sub>, and then volatilize [24], leading to the reduction in the B content in the film.

As a result, the B<sub>4</sub>C layer is deteriorated and degraded. As for the B<sub>4</sub>C/Pd multilayers, the reduction of B atoms leads to the destruction of the periodic structure and the degradation of the optical performance [16,17].

More theoretical and experimental research are required to explore the evolution of the chemical modifications in films. The sample in this study was only a double-layer structure with a thick B<sub>4</sub>C top layer. These structures can be more stable compared with nanoscale multilayer structures in which each layer is only ~1 nm thick [16]. In future, we will investigate the effect of environmental factors, including oxygen and H<sub>2</sub>O, on real B<sub>4</sub>C/Pd multilayers.

## 5. Conclusions

In summary, we explored the stability of B<sub>4</sub>C films and B<sub>4</sub>C/Pd layers placed in a dry nitrogen environment, the atmosphere, a dry oxygen-rich environment, and a wet nitrogen environment. The chemical state of the films was analyzed using XANES, XPS, and FTIR. There was no significant change in the XANES spectra of the single B<sub>4</sub>C films, suggesting that the single B<sub>4</sub>C film was stable even under different environments. In the sample with B<sub>4</sub>C/Pd layers placed in the dry oxygen-rich environment, the XANES spectra demonstrated a significant increase in the  $\pi^*$  states of the B–O bonds and a decrease in the  $\sigma^*$  states in the B–C bonds, indicating that the boron was oxidized and that the B<sub>4</sub>C composition was destroyed under the action of both palladium and oxygen. The XPS results also proved that the amount of oxidized boron in the B<sub>4</sub>C/Pd layers increased due to Pd catalysis. The FTIR results provided the same conclusions as XANES and XPS. These analyses reasonably explain the degradation of the B<sub>4</sub>C/Pd layers in a high-oxygen environment, which should be avoided during storage. This study provides useful guidance for the further development and applications of B<sub>4</sub>C/Pd multilayers.

**Author Contributions:** Conceptualization, Y.F.; methodology, W.L.; software, Y.F.; validation, L.J. and Q.H.; formal analysis, Y.F.; investigation, T.L., G.L. and W.Y.; resources, Z.W.; data curation, R.Q.; writing—original draft preparation, Y.F.; writing—review and editing, L.J., Q.H., Z.Z. and Z.W.; visualization, Y.F.; supervision, R.Q.; project administration, R.Q.; funding acquisition, Z.Z. and Z.W. All authors have read and agreed to the published version of the manuscript.

**Funding:** This research was funded by the National Key R&D Program of China (2016YFA0401304), National Natural Science Foundation of China (61621001), Shanghai Rising-Star Program (19QA1409200), Shanghai Municipal Science and Technology Major Project (2017SHZDZX02), and the Major projects of Science and Technology Commission of Shanghai (No. 17JC1400800). And the APC was funded by National Natural Science Foundation of China (61621001).

**Institutional Review Board Statement:** Not applicable.

**Informed Consent Statement:** Not applicable.

**Data Availability Statement:** No new data were created or analyzed in this study. Data sharing is not applicable to this article.

**Conflicts of Interest:** The authors declare no conflict of interest.

## References

1. Shu, D.; Yun, W. Double Multilayer Monochromator Using a Modular Design for the Advanced Photon Source. *Rev. Sci. Instrum.* **1995**, *66*, 1786. [[CrossRef](#)]
2. Chu, S.Y.; Liu, C. Performance of a Double-Multilayer Monochromator at Beamline 2-BM at the Advanced Photon Source. *Rev. Sci. Instrum.* **2002**, *73*, 1485–1487. [[CrossRef](#)]
3. Riesemeier, H.; Ecker, K. Layout and First XRF Applications of the BAM Line at BESSY II. *X-ray Spectrom.* **2004**, *34*, 160–163. [[CrossRef](#)]
4. Sakurai, K.; Mizusawa, M. Fast X-ray Fluorescence Camera Combined with Wide Band Pass Monochromatic Synchrotron Beam. *AIP Conf.* **2004**, *705*, 889–892. [[CrossRef](#)]
5. Tsuruta, H.; Brennan, S. A Wide-Bandpass Multilayer Monochromator for Biological Small-Angle Scattering and Fiber Diffraction Studies. *J. Appl. Crystallogr.* **1998**, *31*, 672–682. [[CrossRef](#)]
6. Hexemer, A.; Bras, W. A SAXS/WAXS/GISAXS Beamline with Multilayer Monochromator. *J. Phys. Conf. Ser.* **2010**, *247*, 1–11. [[CrossRef](#)]
7. Wang, Y.; Narayanan, S. A Sagittally Focusing Double-Multilayer Monochromator for Ultrafast X-ray Imaging Applications. *J. Synchrotron Radiat.* **2007**, *14*, 138–143. [[CrossRef](#)]
8. Rack, A.; Weitkamp, T. Comparative Study of Multilayers Used in Monochromators for Synchrotron-Based Coherent Hard X-ray Imaging. *J. Synchrotron Radiat.* **2010**, *17*, 496–510. [[CrossRef](#)]
9. Rack, A.; Weitkamp, T. The Micro-Imaging Station of the TopoTomo Beamline at the ANKA Synchrotron Light Source. *Nucl. Instrum. Methods Phys. Res. Sect. B Beam Interact. Mater. At.* **2009**, *267*, 1978–1988. [[CrossRef](#)]
10. Stampanoni, M.; Groso, A.; Isenegger, A. TOMCAT: A Beamline for Tomographic Microscopy and Coherent Radiology Experiments. *AIP Conf. Proc.* **2007**, *879*, 848–851. [[CrossRef](#)]
11. Simon, R.; Buth, G. The X-ray-Fluorescence Facility at ANKA, Karlsruhe: Minimum Detection Limits and Micro Probe Capabilities. *Nucl. Instrum. Methods Phys. Res. Sect. B Beam Interact. Mater. At.* **2003**, *199*, 554–558. [[CrossRef](#)]
12. Rack, A.; Assoufid, L. Hard X-ray Multilayer Mirror Round-Robin on the Wavefront Preservation Capabilities of W/B<sub>4</sub>C Coatings. *Radiat. Phys. Chem.* **2012**, *81*, 1696–1702. [[CrossRef](#)]
13. Dietsch, R.; Rack, A. Performance of Multilayer Monochromators for Hard X-ray Imaging with Coherent Synchrotron Radiation. *AIP Conf. Proc.* **2011**, *1365*, 77. [[CrossRef](#)]
14. Rack, A.; Riesemeier, H.; Vagovic, P. Fully Automated, Fixed Exit, in Vacuum Double-Multilayer Monochromator for Synchrotron-Based Hard X-ray Micro-Imaging Applications. *AIP Conf. Proc.* **2011**, *1234*, 740. [[CrossRef](#)]
15. Hangjian, N.; Qiushi, H. Comparative Study of Pd/B<sub>4</sub>C X-ray Multilayer Mirrors Fabricated by Magnetron Sputtering with Kr and Ar Gas. *Materials* **2020**, *13*, 4504. [[CrossRef](#)]
16. Morawe, C.; Supruangnet, R. Structural Modifications in Pd/B<sub>4</sub>C Multilayers for X-ray Optical Applications. *Thin Solid Film.* **2015**, *588*, 1–10. [[CrossRef](#)]
17. Supruangnet, R.; Morawe, C. Chemical Modification of B<sub>4</sub>C Cap Layers on Pd/B<sub>4</sub>C Multilayers. *Appl. Surf. Sci.* **2016**, *367*, 347–353. [[CrossRef](#)]
18. Qiushi, H.; Yang, L. Nitridated Ru/B<sub>4</sub>C Multilayer Mirrors with Improved Interface Structure, Zero Stress, and Enhanced Hard X-ray Reflectance. *Opt. Express* **2018**, *26*, 21803–21812. [[CrossRef](#)]
19. Yang, L.; Qiushi, H. Thermal and Temporal Stability of the Nitridated Ru/B<sub>4</sub>C Multilayer for High-Flux Monochromator Application. *Appl. Opt.* **2020**, *59*, 48–53. [[CrossRef](#)]
20. Windt, D.L. Reduction of Stress and Roughness by Reactive Sputtering in W/B<sub>4</sub>C X-ray Multilayer Films. *Proc. SPIE Opt. Euv X-ray Gamma-ray Astron. III. Int. Soc. Opt. Photonics* **2007**, *6688*, 66880R. [[CrossRef](#)]
21. Yiwen, W.; Qiushi, H. Nitridated Pd/B<sub>4</sub>C Multilayer Mirrors for Soft X-ray Region: Internal Structure and Aging Effects. *Opt. Express* **2015**, *25*, 7749–7760. [[CrossRef](#)]
22. Zehringer, R.; Künzli, H. Oxidation Behaviour of Boron Carbide. *J. Nucl. Mater.* **1990**, *176–177*, 370–374. [[CrossRef](#)]
23. Li, Y.Q.; Qiu, T. Oxidation Behaviour of Boron Carbide Powder. *Mater. Sci. Eng.* **2007**, *444*, 184–191. [[CrossRef](#)]
24. Viricelle, P.J.; Goursat, P. Oxidation Behaviour of a Boron Carbide Based Material in Dry and Wet Oxygen. *J. Therm. Anal. Calorim.* **2001**, *63*, 507–515. [[CrossRef](#)]
25. Nicolaou, K.C.; Paul, G.B. Palladium-Catalyzed Cross-Coupling Reactions in Total Synthesis. *Angew. Chem. Int. Ed.* **2005**, *44*, 4442–4489. [[CrossRef](#)]
26. Doan, T.T.V.; Wang, J. Theoretical Modelling and Facile Synthesis of a Highly Active Boron-Doped Palladium Catalyst for the Oxygen Reduction Reaction. *Angew. Chem. Int. Ed.* **2016**, *55*, 6842–6847. [[CrossRef](#)]
27. Jun, L.; Junxiang, C. Controllable Increase of Boron Content in B Pd Interstitial Nanoalloy To Boost the Oxygen Reduction Activity of Palladium. *Chem. Mater.* **2017**, *29*, 10060–10067. [[CrossRef](#)]

28. Jiali, W.; Runze, Q. Stress, Roughness and Reflectivity Properties of Sputter-Deposited B<sub>4</sub>C Coatings for X-ray Mirrors. *Chin. Phys. Lett.* **2019**, *36*, 120701. [[CrossRef](#)]
29. Henderson, G.S.; De Groot, F.M.F.; Moulton, B.J.A. X-ray Absorption Near-Edge Structure (XANES) Spectroscopy. *Rev. Mineral. Geochem.* **2004**, *78*, 75–138. [[CrossRef](#)]
30. Yanyan, Y.; Le Guen, K. X-ray Absorption Spectroscopy Study of Buried Co Layers in the Co/Mo<sub>2</sub>C Multilayer Mirrors. *Surf. Interface Anal.* **2017**, *49*, 205–209. [[CrossRef](#)]
31. Xiao, Z.; Zhimin, L. Lithiation-Induced Amorphization of Pd<sub>3</sub>P<sub>2</sub>S<sub>8</sub> for Highly Efficient Hydrogen Evolution. *Nat. Catal.* **2018**, *1*, 460–468. [[CrossRef](#)]
32. Zhihu, S.; Qinghua, L. X-ray Absorption Fine Structure Spectroscopy in Nanomaterials. *Sci. China Mater.* **2015**, *58*, 313–341. [[CrossRef](#)]
33. Zhiming, L.; Yunan, L. Selective Catalytic Reduction of NO<sub>x</sub> with H<sub>2</sub> over WO<sub>3</sub> Promoted Pt-TiO<sub>2</sub> Catalyst. *Catal. B Environ.* **2016**, *188*, 189–197. [[CrossRef](#)]
34. Wensheng, Y.; Qinghua, L. Realizing Ferromagnetic Coupling in Diluted Magnetic Semiconductor Quantum Dots. *J. Am. Chem. Soc.* **2014**, *136*, 1150–1155. [[CrossRef](#)]
35. Liuyang, P.; Runze, Q. Effect of Nitrogen Doping on Surface Morphology, Microstructure, Chemical Composition and Intrinsic Stress of Nickel thin Films Deposited by Reactive Sputtering. *Surf. Coat. Technol.* **2019**, *364*, 196–203. [[CrossRef](#)]
36. Kumar, S.; Infrared, A.K.R. Raman and Electronic Spectra of Alanine: A comparison with Ab Initio Calculation. *J. Mol. Struct.* **2006**, *791*, 23–29. [[CrossRef](#)]
37. Li, D.; Bancrofta, G.M. B K-edge XANES of Crystalline and Amorphous Inorganic Materials. *J. Electron Spectrosc. Relat. Phenom.* **1996**, *79*, 71–73. [[CrossRef](#)]
38. Jiménez, I.; Terminello, L.J. Photoemission, X-ray Absorption and X-ray Emission Study of Boron Carbides. *J. Electron Spectrosc. Relat. Phenom.* **1999**, *101–103*, 611–615. [[CrossRef](#)]
39. Jiménez, I.; Sutherland, D.G.J. Photoemission and X-ray-Absorption Study of Boron Carbide and Its Surface Thermal Stability. *Phys. Rev.* **1998**, *57*, 13167–13174. [[CrossRef](#)]
40. Zhang, D.; Davalle, D.M. The Chemical Composition of As-Grown and Surface Treated Amorphous Boron Carbon Thin Films by Means of NEXAFS and XPS. *Surf. Sci.* **2000**, *461*, 16–22. [[CrossRef](#)]
41. Zhang, D.; Mcilroy, D.N. The Chemical and Morphological Properties of Boron–Carbon Alloys Grown by Plasma-Enhanced Chemical Vapour Deposition. *J. Mater. Sci.* **1998**, *33*, 4911–4915. [[CrossRef](#)]
42. Hsieh, C.H.; Chang, C.H. X-ray Absorption Spectroscopic Study of a Hot Pressed MgB<sub>2</sub>. *Solid State Commun.* **2006**, *137*, 97–100. [[CrossRef](#)]
43. Nan, J.; John, S. High-Energy Electron Irradiation and B Coordination in Na<sub>2</sub>O-B<sub>2</sub>O<sub>3</sub>-SiO<sub>2</sub> Glass. *J. Non-Cryst. Solids* **2004**, *342*, 12–17. [[CrossRef](#)]
44. Nan, J.; Jianrong, Q. Fundamentals of High-Energy Electron-Irradiation-Induced Modifications of Silicate Glasses. *Phys. Rev.* **2003**, *68*, 064207. [[CrossRef](#)]
45. Nan, J.; John, C.H.S. Interpretation of Oxygen K Pre-Edge Peak in Complex Oxides. *Ultramicroscopy* **2006**, *106*, 215–219. [[CrossRef](#)]
46. Ling, H.; Wu, J.D. Electron Cyclotron Resonance Plasma-Assisted Pulsed Laser Deposition of Boron Carbon Nitride Films. *Diam. Relat. Mater.* **2002**, *11*, 1623–1628. [[CrossRef](#)]
47. Bengu, E.; Genisel, M.F. Theoretical and Spectroscopic Investigations on the Structure and Bonding in B–C–N Thin Films. *Thin Solid Film.* **2009**, *518*, 1459–1464. [[CrossRef](#)]
48. Laidani, N.; Anderle, M. Structural and Compositional Study of B–C–N Films Produced by Laser Ablation of B<sub>4</sub>C Targets in N<sub>2</sub> Atmosphere. *Appl. Surf. Sci.* **2000**, *157*, 135–144. [[CrossRef](#)]
49. Moddeman, W.E.; Burke, A.R. Surface Oxides of Boron and B<sub>12</sub>O<sub>2</sub> as Determined by XPS. *Surf. Interface Anal.* **1989**, *14*, 224–232. [[CrossRef](#)]
50. Yue, C.G.K.; Ging, M.N. Identification of Functional Groups and Determination of Carboxyl Formation Temperature in Graphene Oxide Using the XPS O 1s Spectrum. *Thin Solid Film.* **2015**, *590*, 40–48. [[CrossRef](#)]
51. Gar, B.; Hoflund, H.; Hagelin, A.E. ELS and XPS Study of Pd/PdO Methane Oxidation Catalysts. *Appl. Surf. Sci.* **2003**, *205*, 102–112. [[CrossRef](#)]
52. Gabasch, H.; Unterberger, W. In Situ XPS Study of Pd (111) Oxidation at Elevated Pressure, Part 2: Palladium Oxidation in the 10–1 mbar Range. *Surf. Sci.* **2006**, *600*, 2980–2989. [[CrossRef](#)]
53. Bao, R.; Chrisey, D.B. Short Range Order Structure of Amorphous B<sub>4</sub>C boron Carbide Thin Films. *J. Mater. Sci.* **2011**, *46*, 3952–3959. [[CrossRef](#)]
54. HaiYing, C.; Jing, W. Synthesis of Boron Carbide Films by Ion Beam Sputtering. *Surf. Coat. Technol.* **2000**, *128–129*, 329–333. [[CrossRef](#)]
55. Hristov, H.; Nedyalkova, M. Boron Oxide Glasses and Nanocomposites: Synthetic, Structural and Statistical Approach. *J. Mater. Sci. Technol.* **2017**, *33*, 535–540. [[CrossRef](#)]
56. Aoquia, S.-I.; Miyata, H. Preparation of Boron Carbide Thin Film by Pulsed KrF Excimer Laser Deposition Process. *Thin Solid Film.* **2002**, *407*, 126–131. [[CrossRef](#)]